Solid Earth Discuss., 7, 1163–1207, 2015
www.solid-earth-discuss.net/7/1163/2015/
doi:10.5194/sed-7-1163-2015

Solid Earth Discussions
Open Access

The hydrothermal power of oceanic lithosphere

C. J. Grose and J. C. Afonso

ARC Centre of Excellence for Core to Crust Fluid Systems, Department of Earth and Planetary Sciences, Macquarie University, North Ryde, Sydney, NSW 2109, Australia

Received: 19 February 2015 – Accepted: 27 February 2015 – Published: 18 March 2015

Correspondence to: C. J. Grose (christopher.grose@mq.edu.au)

Published by Copernicus Publications on behalf of the European Geosciences Union.

Abstract

We have estimated the power of ventilated hydrothermal heat transport, and its spatial distribution, using a set of recently developed plate models which highlight the effects of hydrothermal circulation and thermal insulation by oceanic crust. Testing lithospheric cooling models with these two effects, we estimate that global advective heat transport is about 6.6 TW, significantly lower than previous estimates, and that the fraction of that extracted by vigorous circulation on the ridge axes (< 1 Ma) is about 50 % of the total, significantly higher than previous estimates. This low hydrothermal power estimate originates from the thermally insulating properties of oceanic crust in relation to the mantle. Since the crust is relatively insulating, the effective properties of the lithosphere are "crust dominated" near ridge axes (yielding lower heat flow), and gradually approach mantle values over time. Thus, cooling models with crustal insulation predict low heat flow over young seafloor, implying that the difference of modeled and measured heat flow is due to the heat transport properties of the lithosphere, in addition to ventilated hydrothermal circulation as generally accepted. These estimates may bear on important problems in the physics and chemistry of the Earth because the magnitude of hydrothermal power affects chemical exchanges between the oceans and the lithosphere, thereby affecting both thermal and chemical budgets in the oceanic crust and lithosphere, the subduction factory, and convective mantle.

1 Introduction

The cooling of oceanic lithosphere over time and distance from ridges is a key constraint on plate tectonics. A predicted consequence of this cooling is that surface heat flux over young seafloor is relatively high and gradually diminishes with age. Although elevated heat flow on average has long been recognized over ridges (Bullard, 1952; Von Herzen, 1959; Von Herzen and Uyeda, 1963; Sclater, 2004), it was also found that measurements are highly scattered. Much subsequent work attempted to explain geo-

SED
7, 1163–1207, 2015

physical observations with models of lithospheric cooling and subsidence, and models were gradually refined by improved constraints on the geophysical properties of the upper mantle (e.g. Langseth et al., 1966; McKenzie, 1967; McKenzie and Parker, 1967; Le Pichon, 1968; Sleep, 1969; Sclater and Francheteau, 1970; Sclater et al., 1971). Eventually, it was recognized that measured heat flow close to ridge axes was far too low to be explained by a model that also explained seafloor subsidence accurately (Sclater and Francheteau, 1970). Following the work of Lister (1972, 1974) and Bodvarsson and Lowell (1972), it became understood that the deficit between measured and predicted heat flow (as well as its scatter) originated in advective hydrothermal ventilation of heat between crustal basement and the oceans. This difference between model and measurement is therefore a proxy to estimating the lithospheric thermal power removed by hydrothermal circulation in oceanic lithosphere. Such constraints on the heat deficit are critically important for the understanding of numerous chemical and physical processes in the Earth. In addition to providing a direct constraint on the thermal budget of cooling oceanic crust and lithosphere (Mottl, 2003; Hasterok, 2013a), this is also the power available to drive chemical exchange between the crust and oceans (e.g., Seyfried et al., 1984; Spivack and Edmont, 1987; Staudigel, 2014), and pass nutrients to sub-seafloor microbial communities (e.g. Jannasch, 1983, 1995; Hessler et al., 1988; Tunnicliffe, 1991). In addition, while dehydration of chemically altered subducting slabs is thought to drive melting in the mantle wedge (Schmidt and Poli, 2013), subduction of altered oceanic crust modulates the secular chemical evolution of the mantle (Ryan and Chauvel, 2013) and volatile cycling between the mantle and hydrosphere may impart a major control on secular changes in the efficiency of mantle convection over Earth history (Crowley et al., 2011).

Although the mentioned heat flow deficit exists in the "unfiltered" global database, Hasterok et al. (2011) and Hasterok (2013a, b) have demonstrated that the deficit is markedly reduced when only marine environments known to have thick sediment cover are considered. Such environments are expected to restrict advective heat transport because hydrothermal ventilation is generally confined to sites of outcropping base-

SED
7, 1163–1207, 2015

ment, and thick sediments reduce the prevalence of outcrops. Moreover, these authors found that a compilation of heat flow estimates from young (< 30 Ma) seafloor with thick sediment cover and extensive geophysical characterization agreed well with conventional lithospheric cooling models (e.g. model GDH1 of Stein and Stein, 1992).

Recently, models of the oceanic lithosphere have been developed that include constraints on the properties of the mantle and crust from mineral physics experiments (Hasterok, 2010; Grose and Afonso, 2013). These models predict that lithospheric heat flow over young seafloor may be significantly lower than that estimated with conventional models. Hasterok (2010) investigated lithospheric cooling models which account for differing properties of crust and mantle. Since the crust is relatively insulating, the effective heat transport properties of the lithosphere are "crust dominated" near ridge axes (yielding lower heat flow), and gradually approach mantle values over time. Also, based on work characterizing crustal accretion and cooling, and hydrothermal heat transport (e.g. Chen and Phipps Morgan, 1996; Cherkaoui et al., 2003), Cochran and Buck (2001) and Spinelli and Harris (2011) showed that hydrothermal transport near ridge axes also results in low heat flow on ridge flanks away from the axis because, after the cessation of hydrothermal advection, the crustal geotherm rebounds from the effects of advective cooling. Finally, the models of Grose and Afonso (2013) showed that axial hydrothermal circulation and crustal insulation together result in a compounded reduction of predicted heat flow in proximity to ridge axes. Since the most robust estimates of net hydrothermal power come from the difference of predicted and measured seafloor heat flow (Mottl, 2003), lower predicted conductive seafloor heat flow suggests that hydrothermal power in oceanic lithosphere must also decrease. The purpose of this paper is to examine these modified predictions of total hydrothermal power, and its spatial distribution, using recent models of lithospheric cooling. We will show that total hydrothermal power may be significantly less than conventional estimates, and that the fraction of hydrothermal power extracted on axis may be up to 50 % of the total. Thus, the extent of off-axis hydrothermal circulation may be less than previously thought. Finally, as the resulting predictions of hydrothermal power (and its implications) depend

SED
7, 1163–1207, 2015

on the accuracy of cooling models, we discuss constraints from global seafloor topography and several regions of young geophysically well characterized seafloor which are thought to constrain the lithospheric heat budget.

2 Methods

2.1 The power deficit

We estimate the power of ventilated hydrothermal circulation Q_H using the conventional difference of predicted and observed heat flow using the equation (e.g. Stein and Stein, 1994):

$$Q_H = \int_0^{t_m} (q_m - q_o) \frac{dA}{dt} dt, \quad (1)$$

where q_m is the modeled heat flow, q_o is the observed heat flow, A is the seafloor area, t is age, and t_m is a maximum integration age. The three key variables are thus the measured and modeled heat flow, and the seafloor area-age distribution. We take the area-age distribution from the empirical model of Muller et al. (2008). The observed heat flow is based on the raw global heat flow database updated by Hasterok (2010). Due to biases in the heat flow database, we employ select filters to ensure that the data better represents the average behavior of the lithosphere. To avoid sampling sites of focused hydrothermal venting we filter out all heat flow values $> 3000\,W\,m^{-2}$. We also remove high-resolution heat flow surveys with dense sampling over young seafloor with extensive thick sediment cover (e.g. Hobart et al., 1985; Davis et al., 1997, 1999) and an anomalous sampling of a mud volcano in the Barents sea (Kaul et al., 2006). Also, all points for which seafloor age cannot be determined are removed. Hasterok (2013b) employed additional filters, including a thermal rebound correction for sediment thickness, and the removal of seafloor area with large igneous provinces. We do

SED
7, 1163–1207, 2015

not include these for reasons of simplicity, our uncertainty in the accuracy of the thermal rebound correction (which increases measured heat flow) and the possibility of other unaccounted corrections which would decrease measured heat flow or systematically increase predicted heat flow (e.g. thermal properties of sediment cover, internal heating sources, or non-plate-like reheating phenomena). Moreover, the thermal correction for sedimentation more strongly impacts observations over old seafloor, where hydrothermal ventilation is probably unimportant. Nevertheless, we will compare our results with those of Hasterok (2013b) to highlight the differences which ought to originate in our respective methodological choices.

2.2 Statistical analysis

Similar to Hasterok (2013b), we perform a non-Gaussian statistical analysis to estimate uncertainties in heat flow and the power deficit. Heat flow measurements are divided into 1 Ma bins and we construct cumulative distribution functions (CDF's) of heat flow for each bin. To estimate the power deficit via Eq. (1) we randomly sample the heat flow CDF once for each bin and sum the deficit to a maximum age t_m of 100 Ma as

$$Q_H = \sum_{t=\Delta t}^{\Delta t/t_m} (q_m - \hat{q_o}) A_{\Delta t}, \quad (2)$$

where $\hat{q_o}$ is the randomly sampled heat flow in the bin, Δt is the bin time interval (1 Ma), and $A_{\Delta t}$ is the total seafloor area in the bin. q_m for the bin uses the mean over the time interval. To obtain probability density functions (PDFs) of hydrothermal power this integration is repeated 10^6 times and we record PDFs for $t_m = 1, 2, 3, \ldots, 100$ Ma. Probability density functions and model predictions of heat flow are shown in Fig. 1a, and CDF's constructed by our analysis are shown in Fig. 1b.

SED
7, 1163–1207, 2015

2.3 Reference models for seafloor heat flow

For plate and half-space models, the relationship between thermal properties of the lithosphere and seafloor heat flux may be given as

$$q_{sf}(t) = [\rho C_p]_{ei}(t)\Delta T_{ei}(t)\sqrt{\frac{D_{ei}(t)}{\pi t}} + q_a, \quad (3)$$

where $[\rho C_p]$ is the volume heat capacity, ΔT is the difference of mantle and surface temperature, D the thermal diffusivity, and q_a is the adiabatic part of the heat flux. The subscript ei denotes that the properties are "transient effective" properties: They are "effective" properties because they are weighted in terms of the depth-integrated change in temperature of the mantle, and they are "transient" because they are in terms of the instantaneous change in the depth-integrated temperature of the mantle (see Appendices). Moving the time t to the left hand side, we can define the coefficient

$$g(t) = [q_{sf}(t) - q_a]\sqrt{t} = [\rho C_p]_{ei}(t)\Delta T_{ei}(t)\sqrt{\frac{D_{ei}(t)}{\pi}}, \quad (4)$$

which may be referred to as a rate of heat flow diminution over time. This coefficient has been useful to characterize simple lithospheric cooling models (e.g. $g(t < 20\,\text{Ma}) = 510\,\text{mW}\,\text{m}^{-2}\,\text{My}^{1/2}$ for model GDH1, Stein and Stein, 1992) as it is basically a term isolating the thermal coefficients. In addition, this coefficient is also useful for analysis of lithospheric models with complicated heat transport properties. In such cases, the effective thermal properties have a time-dependence, thus yielding a time dependent $g(t)$ coefficient. Subtle variations in these properties is much easier to discern in $g(t)$ than in q_{sf}. Cooling half-space models with no properties that depend on depth will have a constant g value, whereas $g(t)$ for plate models will increase when the plate boundary is sensed, and $g(t)$ will be a continuous function of time for any thermal model with depth-dependent properties.

SED
7, 1163–1207, 2015

We test three models of predicted heat flow, from which we calculate the heat flow deficit. The first plate model we use is from Hasterok (2013a), referred to here as H13. H13 has constant properties and is thus taken as an optimal model prediction when the effects of thermal insulation and hydrothermal circulation are not considered. H13 has been constrained based on heat flow data only, and predicts heat flow nearly equal to GDH1 (Stein and Stein, 1992) for ages < 50 Ma and slightly higher heat flow at older ages. Since H13 has constant thermal properties it has a diminution coefficient which is constant over young (< 50 Ma) seafloor. The second and third models we consider are from Grose and Afonso (2013), here referred to as GH and GHC. Both GH and GHC have temperature- and pressure-dependent thermal expansivity and thermal conductivity, temperature-dependent radiative thermal conductivity and specific heat, an initial geotherm calculated with an adiabat and latent heat of melting, and 2-D conductive heat transport (for details, see Grose and Afonso, 2013). In particular, however, we use these two models to illustrate the importance of the two properties most relevant for hydrothermal power calculation: crustal insulation and hydrothermal circulation. Model GH has the above properties as well as hydrothermal circulation near the ridge axis, while model GHC has both hydrothermal circulation and a layer of insulating properties representing the oceanic crust (low density, conductivity, and specific heat). Specifically, GH is model RN10, and GHC is model RN10C from Grose and Afonso (2013). Here we use models with mantle potential temperature T_p = 1325 °C.

The key features of models GH and GHC are their strongly variable $g(t)$ coefficients, shown in Fig. 2. All models have been constrained with old-age seafloor heat flow but, due to the effects of axial hydrothermal circulation and crustal insulation, $g(t)$ (and thus heat flow) deviates significantly over young ages. Thus, comparing predictions of the above three models should illustrate the consequences of axial hydrothermal circulation and crustal insulation on total hydrothermal power, and its spatial distribution.

SED
7, 1163–1207, 2015

2.4 Spatial power distribution

We refer to the deficit integrated to 1 Ma as the near-axial deficit. This deficit may be further divided into active and ridge flank fluxes. The active flux is the hydrothermal power over the ridge axis which is driven primarily by the emplacement and cooling of melts in the crust (Lister, 1982). For cooling models GH and GHC, hydrothermal circulation is modeled using a Nusselt number approximation (e.g. Cochran and Buck, 2001; Spinelli and Harris, 2011), so that the effective thermal conductivity in crust where $T < 800\,^{\circ}\mathrm{C}$ is 10 times the lattice value (plus a radiative contribution). In these models active circulation is extinguished at 0.2 Ma. While model H13 is a simple conductive plate model, we use 0.2 Ma as a cutoff value to estimate the active flux for this model also. After 0.2 Ma, advective transport ceases and the geotherm is in a state of conductive rebound (Cochran and Buck, 2001; Spinelli and Harris, 2011).

To obtain the active deficit we calculate the fraction of heat loss in the 0–0.2 Ma bin as

$$N_{\mathrm{A}} = \int_0^{0.2} q_{\mathrm{m}}\mathrm{d}t \Big/ \int_0^{1.0} q_{\mathrm{m}}\mathrm{d}t \tag{5}$$

where the integral bounds are ages in Ma. From here the active flux Q_{A} is simply $Q_{\mathrm{A}} = N_{\mathrm{A}}Q_{\mathrm{H}}$ (t = 1 Ma), and the ridge flank flux is $Q_{\mathrm{F}} = (1 - N_{\mathrm{A}})Q_{\mathrm{H}}$ (t = 1 Ma). N_{A} values for models H13, GH, and GHC are 0.435, 0.852, and 0.829, respectively. N_{A} values are higher for model GH and GHC due to high q_{m} from hydrothermal circulation. It may be suspected that a correction is needed for the change in observed heat flow between 0–0.2 Ma and 0.2–1.0 Ma, however inspection of the data (not shown) indicates that the heat flow distribution does not change significantly, and is a small fraction of that predicted in any case. Thus our calculations assume that observed heat flow is the same over the entire width of the 1 Ma bin (as it is for all bins).

Finally, the "passive" power deficit is ventilated hydrothermal transport driven by heat conducted into an upper crustal aquifer (Lister, 1982), resulting in long term convective

SED
7, 1163–1207, 2015

fluid exchange between the crust and oceans. The passive power deficit is the total power deficit after subtraction of the near-axial deficit: $Q_P = Q_H(60\,\text{Ma}) - Q_H(1\,\text{Ma})$.

3 Results and discussion

Figure 3 shows the main results of our analysis of the heat flow deficit for different cooling models. PDF's of the time-integrated power deficit are plotted (Fig. 3a–c) for maximum integration times between 1 and 60 Ma. Since the heat flow sampling is divided into 1 Ma bins, the PDF for the power deficit at 1 Ma is essentially the derivative of a single CDF and thus appears rough. Nevertheless, the modes (probability maxima) are well defined for all ages. For comparison, the means and medians of the PDF's are also calculated for each age. The resulting PDF's have non-normal distributions, as the low probability realizations are skewed to low power estimates. For a different visualization, the mean, median, mode, and half-maximum bounds (HMB) of the power deficit are also plotted as a function of age up to 100 Ma in Fig. 3d–f. This shows that the net deficit plateaus around 50 Ma for all models, where predicted and observed heat flow converge (Fig. 1).

3.1 The net power deficit

3.1.1 Model H13

For model H13, our analysis predicts that the net power deficit is 7.8 TW, with half-maximum realizations falling between 3.8 and 10.1 TW. Compared to most previous studies (e.g. Sclater et al., 1980; Stein and Stein, 1994; Stein et al., 1995; Mottl, 2003; Spinelli and Harris, 2011) this is a low estimate. The estimates of 10.3 and 11.5 TW by Sclater et al. (1980) and Stein and Stein (1994), respectively, are even outside of the HMB for this cooling model. As model H13 is nearly equivalent to GDH1 (Stein and Stein 1992), the difference is related to the heat flow database, seafloor area-age distribution, and statistical treatment. In addition, our mean (6 TW) and median

SED
7, 1163–1207, 2015

(6.6 TW) net power deficit estimates are even lower than the mode (Fig. 3a). Although they are within the HMB, they are substantially lower than previous estimates.

It is notable that our estimate of 7.8 TW for H13 is equal to that estimated by Hasterok's (2013b) analysis using his filtered heat flow database. However, this is only coincidental as his filtered database removes seafloor with sediment thickness > 400 m, whereas we do not include such a filter. Moreover, even the more comparable "unfiltered" database of Hasterok (2013b) incorporates additional corrections not employed here including (1) a thermal rebound correction for sediment thickness, (2) removal of seafloor area with large igneous provinces, and (3) median reference model heat flow q_m was used (we use means). With these additional corrections, Hasterok (2013a) predicted a net power deficit of 6.2 TW. As such, our method predicts a roughly 25 % greater net power deficit. Therefore, if Hasterok's (2013b) database and analytical techniques are preferred, our net deficit estimates should be reduced by 20 %, or slightly less than our median estimates.

3.1.2 Models GH and GHC

The power deficits for thermal plate models GH and GHC are shown in Fig. 3b and c. Model GH predicts a power deficit of 10 TW, with half-maximum realizations falling between 6.1 and 12.3 TW. This value is in good agreement with many previous estimates of the power deficit as discussed above. Inspection of Fig. 2 shows that predicted heat flow for GH and H13 is similar except near the ridge where GH heat flow becomes lower than H13. Thus the high heat flow deficit for model GH originates in active hydrothermal transport on ridge axes. Model GH predicts 4–14 $W m^{-2}$ for < 0.2 Ma.

Model GHC has similar properties to GH, except that GHC has an insulating oceanic crust, and all heat transport properties are allowed to vary from their experimental values in order to fit basin-scale geophysical observations (Grose and Afonso, 2013). The predicted net power deficit of model GHC is substantially lower than GH. We estimate 6.6 TW, with half-maximum bounds of 2.9 and 8.8 TW (Fig. 3c). Thus, if normal lithospheric cooling is better modeled by GHC, then the net power deficit is about 35 %

SED
7, 1163–1207, 2015

lower than expected by model GH. Note, however, that this does not mean that the effect of crustal insulation is a 35 % decrease. This is because, again, the differences between model GH and GHC are both crustal insulation and a re-adjustment of all mineral physics properties to best fit geophysical observations. Since the effective thermal conductivity of model GHC is adjusted to be ∼ 10 % higher than GH (see Grose and Afonso, 2013), the real effect of crustal insulation on the heat flow deficit is closer to a 45 % reduction.

3.2 Spatial distribution of the power deficit

3.2.1 Model H13

The spatial distribution of hydrothermal power predicted by models H13, GH, and GHC are highlighted at the top of their respective panels in Fig. 3a–c, and are tabulated in Table 1. For H13, the power deficit at 1 Ma has a probability maximum at 2.5 TW with HMB between 1.9 and 2.8 TW (approximated after smoothing due to PDF roughness). The cumulative near-axial deficit is 32 % of the total. This may be divided into power on the ridge axis (0–0.2 Ma) at 14 % of the total, and 18 % of the total on ridge flanks (0.2–1.0 Ma). The remaining deficit of 5.3 TW (68 % of the total) is due to passive ventilated hydrothermal circulation away from ridges. This prediction of 32 % of total hydrothermal power occuring over < 1 Ma crust is only slightly higher than most previous estimates. Stein and Stein (1994) predict a 28 % near-axial deficit, Pelayo et al. (1994) predict about 23 %, and Mottl (2003) predicts 29 % occurring near the axis (Table 1). In addition to the use of an updated heat flow database, our slightly higher value may be attributed to our preference to modes rather than the means (Table 1). Using mean values, we calculate a near-axial power deficit closer to 20 % of the total. This is slightly lower than Spinelli and Harris's (2011) prediction that 25 % of the deficit occurs over near-axial seafloor (using Eq. 1 on a conduction-only model).

SED
7, 1163–1207, 2015

3.2.2 Models GH and GHC

As shown in Fig. 3b and c and Table 1, both models GH and GHC predict that about 50 % of total hydrothermal power is extracted near ridge axes (< 1 Ma). To our knowledge, this is a higher fraction than all previous estimates, including Spinelli and Harris' (2011) near-axial estimate of 40 %. Moreover, about 85 % of the axial deficit (40–45 % of the total) is active circulation on < 0.2 Ma seafloor. For model GH, the near-axial deficit (5.2 TW) and the active deficit (4.4 TW) are high, leaving about 4.8 TW to drive passive circulation. On the other hand, because the net power estimate of model GHC is significantly lower than GH, the near-axial power estimate (< 1 Ma) and the passive regime estimate are both only 3.3 TW. For the near-axial environment, this estimate is in good agreement with some previous investigators (e.g. Stein and Stein, 1994; Mottl, 2003; Spinelli and Harris, 2011; Table 1), but this passive estimate is much lower than previous estimates (Table 1). Some passive power estimates are more than twice our value (e.g. Stein and Stein, 1994; Pelayo et al. 1994; Mottl, 2003). The low passive power estimate for GHC originates primarily in the compounding effects of thermal rebound from active hydrothermal circulation and thermal insulation of oceanic crust. The hydrothermal model from Spinelli and Harris (2011) predicted a passive power budget of 5.4 TW, about 60 % higher than our estimate for model GHC (Table 1). Hasterok's (2013b) passive estimate of 3.9 TW is closest to our result. However, this value is for his 'unfiltered' database which predicted a total deficit of 6.2 TW (Table 1). If we used similar methods, we estimate that predictions for model GHC would be about 20 % lower, with a passive deficit of ~ 2.6 TW and total deficit of ~ 5.3 TW (80 % of 6.6 TW).

4 Heat flow constrained by topography

Our analysis has shown that insulating oceanic crust and hydrothermal circulation jointly impact estimates of hydrothermally mined energy in oceanic lithosphere, as well as its spatial distribution. This occurs because both effects result in the prediction of

SED
7, 1163–1207, 2015

significantly lower heat flux over young (< 30 Ma) seafloor compared to conventional models (Fig. 2), and active hydrothermal circulation elevates heat flow on ridge axes. Clearly, an important question is whether or not observations actually support lower heat flow over young seafloor. Although measured seafloor heat flow is contaminated by ventilated hydrothermal circulation processes, other geophysical observations such as seafloor subsidence may be robust alternative constraints on lithospheric heat loss (Parsons and McKenzie, 1978; Sandwell and Poehls, 1980; Wei and Sandwell, 2006).

Hofmeister and Criss (2005), based on the assumption that classical lithospheric cooling models do not fit the Earth, and advective processes were not responsible for low heat flow over young seafloor, suggested that true heat loss from oceanic lithosphere is that actually measured (~ 20 TW, versus ~ 30 TW, Von Herzen et al., 2005). Wei and Sandwell (2006) attempted to show that although measured heat flow does not match lithospheric heat loss as predicted by plate models, it is reflected in the rate of seafloor subsidence. Wei and Sandwell (2006) calculated seafloor heat flow based on a spatial integration of heat flows estimated by local subsidence rates found with the global seafloor depth grid of Smith and Sandwell (1997) and age grid of Muller et al. (1997). They calculated local seafloor heat flux by employing the equation

$$q_{\mathrm{sf}} - q_{\mathrm{a}} = \frac{\rho C_p}{\alpha \varrho} \frac{\nabla t(x,y) \cdot \nabla w}{\nabla t(x,y) \cdot \nabla t(x,y)} \tag{6}$$

where $t(x,y)$ is the age as a function of spatial coordinates, q_{a} is an additional heat flux which is extracted from sub-lithospheric mantle rather than the lithosphere (e.g. the adiabat), and

$$\varrho = \frac{\rho_{\mathrm{b}}}{\rho_{\mathrm{b}} - \rho_{\mathrm{w}}} \tag{7}$$

is the isostatic correction for seawater load, with mantle density ρ_{b} and seawater density ρ_{w}.

Although they found that their heat flux calculations were in good agreement with a simple half-space cooling model (where $g = 420\,\mathrm{mW\,m^{-2}\,s^{1/2}}$) and conventional net

SED
7, 1163–1207, 2015

seafloor heat flux estimates, this agreement only occurred upon addition of a hidden lithospheric heat flux, q_a, of 38 mW m^{-2}, or about 11 TW. Consequently, the analysis of Wei and Sandwell (2006) suggested that an empirical subsidence-based estimate of net seafloor heat flux is on the order of 20 TW, in agreement with Hofmeister and Criss (2005).

We suggest that the solution to this dilemma lay in the age-dependence of the effective thermal properties (Appendix B). For example, Goutorbe (2010) and Grose (2012) found that simple thermal plate models with temperature-dependent thermal properties (i.e., no dependence on age), optimally fitted to geophysical observations, required an effective thermal expansivity about 30–40 % lower than the experimental value for olivine. Since Wei and Sandwell (2006) perform no ad hoc adjusments to thermal properties, their use of high thermal expansivity resulted in a low seafloor heat flux and an 11 TW addition of heat was necessary for a reasonable result.

Consider that, similar to Eq. (6), seafloor heat flow and subsidence may be related by the equation (Appendix A)

$$\frac{b_{ei}(t)}{2\varrho(t)\alpha_{ei}(t)} = \frac{g(t)}{[\rho C_p]_{ei}(t)} \tag{8}$$

where $b_{ei} = \mathrm{d}w/\mathrm{d}\sqrt{t}$ is the transient subsidence rate with w the seafloor depth, and α_{ei} the transient effective thermal expansivity. The age-dependence in the rate of heat flow diminution $g(t)$ is shown for our models GHC and GC, and Hasterok's (2013) model H13, in Fig. 2b. While our predictions are not as low as that measured, as expected by Hofmeister and Criss (2005), the difference between model and measurement is significantly lower than that estimated with simple plate models. Since this decrease is only partially compensated by high heat flow on ridge axes, the power transported by hydrothermal circulation is also markedly reduced. Accordingly, the problem of the heat flow deficit can be attributed to both complex thermal properties and advective transport.

SED
7, 1163–1207, 2015

4.1 The subsidence rate

Age-dependence of the subsidence rate, as predicted by GDH1 (Stein and Stein, 1993), H13 (Hasterok, 2013a), and our models GH and GC are shown in Fig. 4 compared to empirical estimates based on the global database of Hillier (2010). The empirical estimates are obtained from fitting a line (least squares fit) through the data (0.1 My bins) in a sliding window of width $\delta t^{1/2}$. To explore the sensitivity of estimates to the sampling window size we show estimates for $\delta t^{1/2}$ between 0.2 and 2.0 $\mathrm{My}^{1/2}$. Due to the roughness of the data in small bins, the variance is high when the window is small and decreases as the window becomes larger.

Comparison of model predictions and empirical estimates shows that model GH and GHC both fit the general trends in almost all of the data well, while models H13 and GDH1 substantially over-predict subsidence rates for the youngest lithosphere (< 4 Ma). Model H13 does not fit the data well because it was fit to the depth curve predicted by the model of McKenzie et al. (2005), but we include it for completeness. The empirical subsidence rate clearly has a rising trend between near-zero age and about 30 Ma, then decreases gradually in accordance with seafloor flattening. It is notable that empirical estimates using large $\delta t^{1/2}$ tend to rise near zero age and thus appears to be in better agreement with model GH rather than GHC. However, this is due to the axial rise present over much of the Earth's fast spreading seafloor, and model GHC is a superior fit to ridge flank subsidence. The estimates with $\delta t^{1/2} \sim 0.2\,\mathrm{My}^{-1/2}$ indicate that the subsidence rate is $\sim 150\,\mathrm{m\,My}^{-1/2}$ near the ridge axis (~ 0.5 Ma), increases to $\sim 350\,\mathrm{m\,My}^{-1/2}$ around 30 Ma, and finally decreases gradually from the effects of seafloor "flattening" to great age.

Although the data better fit model GHC rather than model GH, both models fit the data well, given the manner in which the empirical estimates vary and undulate with age.

SED
7, 1163–1207, 2015

5 A constraint from the thermal budget of crustal cooling

Based only on the fit to the global data, we cannot discount the possibility that crustal insulation is an unimportant contribution. On the other hand, we may cast doubt on the feasibility of model GH for a thermodynamic reason, thus requiring a contribution from crustal insulation.

It is notable that the estimate of near-axial circulation for model GH is so high (5.2 TW, Table 1). Based on the limited heat budget for ocean crust formation and cooling, Mottl (2003) argued that axial cooling cannot be more than about 3.1 TW. This indicates that model GH, due to high effective thermal conductivity and axial boundary conditions around the shallow axial magma chamber (Grose and Afonso, 2013), may be extracting more heat than can realistically be released by advection and crystallization of magmas. Model GHC, on the other hand, only transports about 3.3 TW of heat, consistent with Mottl's arguments. In addition, Grose and Afonso (2013) showed that model GHC predicts ridge thermal structure that is in good agreement with a seismic model over the East Pacific Rise by Dunn et al. (2000). As this fit to a seismic model reflects the Nu number, the seismic model supports the choice of Nu $\approx$ 10 rather than significantly higher values suggested elsewhere (e.g. Cochran and Buck, 2001; Spinelli and Harris, 2011). On the other hand, Han et al. (2014), based on the observation of off-axis magma lenses in regions Dunn et al. expected to be cool, suggested that Dunn's model may be inaccurate. However, it is not clear what ambient thermal structure is consistent with the presence of off-axis magma lenses, as these may be anomalous, even if frequent, features. We stress that models GH and GHC use a simple Nu-number approximation of hydrothermal transport, and therefore can only represent the average behavior of ridges both along and across axes. Moreover, if the thermal structure of Dunn et al. (2000) is too cold, the necessary adjustments to model GHC may be small, except in direct proximity to the axial magma lens. Such corrections may also be applied to model GH, but they will be larger, and may be at the cost of good fit to seafloor subsidence.

SED
7, 1163–1207, 2015

In summary, if there is no effect of crustal insulation, the fit to seafloor subsidence is slightly compromised and unrealistic amounts of heat are extracted on axis. Thus, we suggest that both insulating oceanic crust and a moderate amount of axial hydrothermal circulation are important for estimates of hydrothermal power.

6 High-resolution heat flow surveys

When sediment cover is sufficiently extensive so as to act as an impermeable boundary over the crust, fluid exchange is no longer effective and heat transfer occurs by conduction (Lister, 1972). Thus, one approach to retain the use of heat flow to constrain lithospheric cooling is to remove regions with thin sediment cover from the heat flow database. Such an analysis has been performed by Hasterok et al. (2011) and Hasterok (2013b). These authors showed that for regions with sediment cover > 400 m, measured heat flow is in good agreement with model H13 (and GDH1) for ages > 25 Ma. However, for younger ages there still remains a substantial heat flow deficit (Fig. 2), indicating that a signal of ventilated circulation persists for < 25 Ma seafloor, or the models overpredict heat flow.

An additional approach is to examine specific sites that are studied extensively enough to demonstrate that effects of ventilated hydrothermal circulation are small or can be properly culled. Among the global data, Hasterok et al. (2011) recognized four sites on young seafloor which have thick sediment cover and have been extensively surveyed. These include the Juan de Fuca ridge flank (Davis et al., 1997, 1999), the Costa Rica Rift flank (Davis et al., 2004; Hobart et al., 1985; Langseth et al., 1988), the Gulf of Aden (Cochran, 1981; Lucazeau et al., 2008; 2010), and the Cocos plate (Hutnak et al., 2008). Heat flow estimates from these sites are plotted in Fig. 2 and are discussed below.

SED
7, 1163–1207, 2015

6.1 Juan de Fuca ridge

The Juan de Fuca ridge flank is the most extensively surveyed ridge with over 1000 heat flow measurements collocated with seismic reflection profiles (Hasterok et al., 2011). However, much of the data is not suitable as a basis for determining lithospheric heat flow since many areas are strongly effected by hydrothermal ventilation. An extreme example of this is the study by Wheat et al. (2004) which looked at a site of focused venting along a fault, where measured heat flow is on the order of tens of $W m^{-2}$. On the other hand, the Endeavor segment of the Juan de Fuca plate is heavily sedimented and has been extensively studied with collocated heat flow (Davis et al. 1997, 1999), seismic reflection profiles (Rosenberger et al., 2000), and geochemical study from nine ODP boreholes (Elderfield et al., 1999) over a 80 km transect in the direction of spreading. Heat flow measurements are shown in Fig. 2. Note that measurements cluster around 1 and 3.6 Ma. The scattered black line is an empirical calculation based on the relationship between sediment thickness, basement temperature, and surface heat flow (Davis et al., 1999). Davis et al. (1999) estimated that a sediment correction of +15 %, was necessary to estimate basement heat flow. However, we use the +6 % correction from Pribnow et al. (2000) which accounts for thermal anisotropy of sediment. As the data are scattered we calculate distance-weighted averages of heat flow from the measurements for ages (A) 0.66–1.56 Ma, (B) 1.0–1.56 Ma, and (C) 3.34–3.6 Ma. The difference between average A and B is that average A uses the low heat flow "tail", whereas average B cuts off these low measurements.

Overall, the Juan de Fuca data seem to best fit model GH. However, the average heat flow at 3.5 Ma is in between models GH and GHC, and it is appropriate to include the low heat flow "tail" at ages < 1.0 Ma, then average heat flow around 1 Ma is in good agreement with model GHC. The low heat flow at < 1 Ma and high heat flow at 1.3 Ma indicates that the region is significantly influenced by advective transport in a basement aquifer. The conventional hydrogeological interpretation of heat flow along the Endeavor flank includes recharge over the young (< 0.66 Ma) unsedimented seafloor

SED
7, 1163–1207, 2015

and discharge at a basement high around 1.3 Ma, about 20 km from the recharge site (Davis et al., 1997, 1999; Newman et al., 2011). Elevated heat flow in this region may be explained by (1) spatial sampling bias, (2) a source of additional heat flow, or (3) different properties of the lithosphere than expected by model GHC. Different properties may either be a regional difference, or a global difference, ruling out model GHC. Possible sources of elevated heat flow are (1) continued deep hydrothermal circulation, perhaps associated with faulting as suggested by Nedimovic et al. (2009), (2) heat release from hydration of the crust (Lowell and Rona, 2002), (3) heat transported from younger seafloor and discharged, consistent with models (Davis et al., 1997, 1999; Newman et al., 2011), or (4) microbial thermogenesis, which is difficult to quantify, but could be significant if nutrient supplies are adequate (D. LaRowe, personal communication, 2012).

6.2 Costa Rica Rift: heat flow

The geophysical environment of ~ 6.5 Ma seafloor around ODP Hole 504B on the Costa Rica Rift (CRR) has been characterized with a high resolution (~ 1 km spacing) gridded survey of heat flow (Davis et al., 2004; Hobart et al., 1985; Langseth et al., 1988) and seismic reflection profiles (Swift et al., 1998). Figure 5a shows a sediment thickness map produced from the seismic reflection profiles (12 545 points) and a bicubic spline. Figure 5b shows a bicubic spline of heat flow. Inspection of Fig. 5a and b shows that there is some correlation between sediment thickness and heat flow, although the relationship is rough (Swift et al., 1998). Using only the measurements, heat flow for the region has a mean of 229 ± 46 (1σ uncertainty) and median of 218 (194, 250) $\mathrm{mW\,m^{-2}}$ (interquartile range uncertainty). However, since measurement coverage has a greater density around sites of elevated heat flow and thin sediment cover the statistics are biased to elevated values. The statistics for the bicubic spline are shown as a probability density function in Fig. 5c, which are also compared to a more coarse PDF for the measurements alone. The mean of the spline is $211 \pm 35\,\mathrm{mW\,m^{-2}}$, the median is 203 (186, 229) $\mathrm{mW\,m^{-2}}$, and the mode is 190 $\mathrm{mW\,m^{-2}}$ (173, 217) (half-

SED
7, 1163–1207, 2015

maximum uncertainty). If we consider that sampling coverage is extensive enough to cover spatial heterogeneity, the mean of the spline may be preferred. However, we note that there are many areas where closely spaced points reveal exceptional lateral gradients, even away from areas of thin sediment or evidence of anomalies in basement topography (Fig. 5). Moreover, recall that measurements on the Juan de Fuca flank have a much smaller spacing (~ 250 m) and show substantial scatter. A similar scatter may be normal for the CRR site, so that the mean of the spline may not accurately characterize the true mean. We thus take the mode of the spline as the lowest reasonable statistical tendency.

6.3 Costa Rica Rift: normal seafloor?

The mode and its uncertainty are plotted for the CRR in Fig. 3. This estimate is in good agreement with models GH and H13. However, it is significantly higher than that predicted by model GHC (~ 170 mW m^{-2} at 6 Ma). But does the CRR consist of "normal" seafloor? In other words, compared to the thermal conditions of model GHC, is there an additional property of this region which, if accounted, would elevate lithospheric heat flow by about 20 %? There are at least two properties of the region worth considering. The first is that the thickness of oceanic crust has been constrained to be ~ 5 km, significantly thinner than other examples of seismically normal oceanic crust (Becker et al., 1989). Thus, the crustal insulation effect in this region should be lower. We have tested this by performing a sensitivity analysis with model GHC where the thickness of the insulating layer is varied between 0 and 10 km (Fig. 6). The model GHC with a 5 km thick crust, or GHC-CRR, predits heat flow > 180 mW m^{-2}. This is better agreement, although it remains barely within the lower bound of uncertainty using a somewhat generous statistical technique. To find the maximum possible conductive heat flow we test the predictions of GHC after hydrothermal circulation is removed (red line). This can increase the heat flow nearly to the value of the mode, although this is a maximum. Note that model GH predicts lower heat flow than model GHC with no hydrothermal circula-

SED
7, 1163–1207, 2015

tion and no oceanic crust because model GH has different lithospheric heat transport properties.

In addition, there may be the possibility that the CRR has been effected by the Galapagos hotspot. Figure 7 shows a paleoridge reconstruction from Wilson and Hey (1995) based on a constant rate of Nazca-hotspot motion. The present distance between Hole 504B and the hotspot centre is about 800 km. At the time of accretion (~ 6.5 Ma) the hotspot was about 600 km from the CRR, and at 8 Ma the distance reduces to about 500 km. Although this is within the limit of the present-day bulge associated with the Galapagos hotspot, migration of plume material may be funneled by ridges, ultimately displacing ambient mantle beneath the CRR. Cooling of this plume material will thus generate lithosphere with plume composition and temperature.

Clear hurdles to the hypothesis of hotspot interaction are that the distance is large, propagation may be limited by fracture zones, Nazca-hotspot motion may tend to drag the plume away from the CRR, and the depth to seafloor at hole 504B is consistent with the depth of normal seafloor at this age (~ 3450 m). This last item may be explained by thin oceanic crust.

6.4 Gulf of Aden

The Gulf of Aden is a rifted margin between Africa and the Arabian plate which separated at 34 Ma with the onset of seafloor spreading around 18 Ma (Leroy et al., 2012). Lucazeau et al. (2010) reported high quality heat flow measurements along 8 seismic profiles near the margin of the Arabian plate (near Dhofar), 7 of which are aligned with the direction of spreading. They correct their heat flow measurements for sedimentation rate (we use the average of their two cases), topography, and heat refraction. These profiles extend from the continental domain, through the ocean-continent transition, and onto oceanic lithosphere. The small variance in heat flow along profiles led Lucazeau et al. (2008) to conclude that effects of hydrothermal circulation are not important. Of their 162 measurements along 8 profiles, we use 40 points from 6 profiles located on seafloor with ages known from magnetic anomalies (d'Acremont et al.,

SED
7, 1163–1207, 2015

2010). Comparison of the model age grid of Muller et al. (2008) and magnetic anomaly isochrons suggests that ages are overestimated by 5–10 Ma near the continental margin. Therefore, we neglect two profiles from seafloor on the East side of the Socotra Hadbeen fracture zone, since we cannot confidently determine precise ages. The 40 measurements are on seafloor 16–17.6 Ma and are plotted in Fig. 3 along with their mean and standard deviation ($114 \pm 10\,\mathrm{mW\,m^{-2}}$).

Although the mean is in best agreement with model GHC, the standard deviation stretches over all 3 models investigated. Despite this agreement, it is likely that this survey examines anomalous seafloor. The site characterizes the early stages of rifting margins, the onset of seafloor spreading, and any thermal consequences of abutting a continental margin. Moreover, based on an examination of heat flow and thermomechanical modeling, Lucazeau et al. (2008) suggested that an intense ($\sim 300\,^{\circ}\mathrm{C}$) thermal anomaly below the ocean-continent transition may be likely. If this is the case, then the reported heat flow values should be elevated above that of normal seafloor. "Correcting" for these effects would be expected to bring predictions in better agreement with model GHC, or a model with even lower heat flow.

6.5 Cocos Plate

Hutnak et al. (2008) performed a regional survey of heat flow over Cocos Plate seafloor with ages 18–24 Ma. The region is blanketed with thick (400–500 m) sediments except for unevenly spaced sites of outcropping basement. Distributed throughout the region are collocated heat flow and seismic-reflection profiles, some of which extend from outcrop sites and others interspersed about. This heat flow survey revealed a bimodal areal variation in surface heat flow for low ($\sim 30\,\mathrm{mW\,m^{-2}}$) and high ($\sim 110\,\mathrm{mW\,m^{-2}}$) heat flow areas, a pattern which the authors explain by low-temperature hydrothermal discharge and recharge among outcrops in the low-heat flow areas, and "warm" hydrothermally inactive crust for the high heat flow areas. Their estimate of 97–$120\,\mathrm{mW\,m^{-2}}$ is plotted in Fig. 3 with the age range 18–24 Ma. This estimate is in best

SED
7, 1163–1207, 2015

agreement with model GHC, although the uncertainty overlaps heat flow predicted by models H13 and GH.

6.6 Summary of high-resolution sites

Overall, the four specific sites discussed above show heat flow elevated above the predictions of the sediment-filtered global database of Hasterok (2013b), and are in rough agreement with all models considered. As previously recognized (Davis et al., 1997, 1999; Lucazeau et al., 2008; Hutnak, 2008; Hasterok et al., 2011), this demonstrates that the low scattered heat flow over young seafloor is due to ventilated hydrothermal circulation, and that careful geophysical characterization can allow the lithospheric heat budget to be at least partially revealed on young seafloor. Heat flow estimates from the Cocos plate (Hutnak et al., 2008) and the Gulf of Aden (Lucazeau et al., 2008, 2010) are in marginally better agreement with model GHC. However, these sites are located on seafloor where predicted heat flow from all models is not significantly different (Fig. 3), and the Gulf of Aden might not be considered "normal" seafloor. The Juan de Fuca ridge flank is geophysically well characterized, but there is strong evidence of ventilated discharge over much of the sampled area (Davis et al., 1997, 1999). The elevated heat flow in this area may reflect this discharge, persistent deep hydrothermal circulation along faults (Nedimovic et al., 2009), heat release from hydration (Lowell and Rona, 2002), or advection from younger seafloor. Heat flow on the Costa Rica Rift is probably the most important datapoint as it (1) samples seafloor young enough to potentially differentiate models, (2) is heavily sedimented with no evidence of focused or off-site advective transport, and (3) is well characterized for heat flow and basement depth. CRR heat flow is higher than our preferred model GHC, but this can be explained as an effect of thin oceanic crust, and possibly a contribution from the Galapagos hotspot.

Unfortunately, since only two sites considered here are located on < 10 Ma lithosphere, it is difficult to judge the validity of any model based solely on heat flow. Using heat flow data to constrain the details of lithospheric cooling may require future

SED
7, 1163–1207, 2015

geophysical surveying efforts targeting well sedimented < 10 Ma seafloor. We thus expect that continued development of our understanding of the relationship between heat loss and seafloor topography may be instrumental (e.g. Parsons and McKenzie, 1978; Sandwell and Poehls, 1980; Wei and Sandwell, 2006). Since heat flux may be calculated if the effective thermal expansivity and volume heat capacity are known (Eq. 8), future efforts should focus on linking detailed models of near-ridge environments (e.g. Cherkaoui et al., 2003; Maclennan, 2008; Craft and Lowell, 2009; Theissen-Krah et al., 2011) with comprehensive mineral physics and hydrogeological models of the lithosphere (e.g. Afonso et al., 2007, 2008; Hasterok, 2010; Goutorbe and Hillier, 2013; Grose and Afonso, 2013).

7 Conclusions

We have estimated the power of ventilated hydrothermal heat transport, and its spatial distribution, using a set of recent plate models which highlight the effects of hydrothermal circulation and crustal insulation. The most important conclusion of our study is that a model with both of these effects predicts that the difference between measured and modeled heat flow is significantly lower than previously thought. Consequently, the total heat vented to the oceans by hydrothermal circulation is lower, and the fraction of that vented is higher on ridge axes.

Our hydrothermal power estimate for a model with constant thermal properties is similar to the recent analysis of Hasterok (2013a), predicting a net power deficit of 7.8 TW, 34 % of which is extracted near the ridge axis (< 1 Ma). The effect of axial hydrothermal circulation alone is a higher net power deficit (10 TW), and about 50 % of the hydrothermal heat flux occurs near ridge axes (< 1 Ma). Finally, the effect of crustal insulation with hydrothermal circulation is a markedly lower net power deficit (6.6 TW), with no relative change to the heat flow distribution (50 % near the axis). If median or mean estimates are preferred against probability maxima, total hydrothermal power estimates are about 10 or 20 % lower than these estimates, respectively.

SED
7, 1163–1207, 2015

Many physical and chemical processes in the Earth may be affected by the above predictions. As less heat is transported by hydrothermal circulation, this may also imply that less fluid is circulated in the crust, or that such fluids have a lower average temperature. The lower off-axis advective heat flux also suggests that off-axis "diffusive" hydrothermal circulation is not as vigorous as previously thought. These reduced energy constraints must affect chemical exchanges between the crust and oceans, including the passing of nutrients to subseafloor microbial communities and the alteration of oceanic crust. In turn, these effects should impact chemical budgets in the subduction factory and the secular chemical evolution of the mantle. Also, the crustal insulation effect may have broader implications for the thermal evolution of the Earth. Crustal insulation reduces the present day global heat flux by about 2–3 TW. This reduction will multiply into the past as a warm mantle generates systematically thicker crust and greater insulation.

Finally, the important question remains: do the cooling models represent the Earth accurately? With this question in mind, we have studied model fits to empirical estimates of seafloor subsidence and geophysically well characterized sites of heat flow measurements. While a model with both hydrothermal circulation and crustal insulation (GHC) best fits global average seafloor subsidence, site-specific heat flow can be explained with a model which does not include crustal insulation (GH). Additional detailed heat flow surveys of < 10 Ma seafloor will be helpful in the choice of best models on the basis of heat flow. The heat budget of cooling oceanic crust, however, is in best agreement with model GHC, as model GH predicts a probably unrealistic extraction of energy on the ridge axis. Accordingly, we find that the cooling regime of the near-axial environment and basin-scale oceanic lithosphere is best explained by models with insulating oceanic crust.

SED
7, 1163–1207, 2015

Appendix A: Subsidence-heat flux relation

The usual definition of the (net) seafloor subsidence rate b_e is

$$b_e(t) = \frac{h(t) - r}{\sqrt{t}} = \frac{w(t)}{\sqrt{t}}, \tag{A1}$$

where $h(t)$ is the seafloor depth, r is the ridge height, $w(t)$ is the net subsidence, and t is the age. A corresponding solution to Eq. (A1) for half-space cooling models can be given as

$$b_e(t) = 2\varrho(t)\alpha_e(t)\Delta T_e\sqrt{\frac{D_e(t)}{\pi}}, \tag{A2}$$

where ΔT_e is the effective difference of mantle and surface temperature, α_e the effective thermal expansivity, and D_e the effective thermal diffusivity. Because many of these properties change as a function of depth, the "effective" values for the lithosphere, and thus the seafloor subsidence rate, have a complicated dependence on time. On the other hand, conventional models with constant properties (or at least no depth-dependent properties) predict a constant subsidence rate. Equations (A1) and (A2) characterize the net subsidence rate, which is a function of the entire cooling history. It is essentially the slope of a line in $t^{1/2}$ between depth $r = w(t = 0)$ and $w(t)$. We may also describe the transient, or instantaneous, subsidence rate as

$$b_{ei}(t) = \frac{\mathrm{d}w}{\mathrm{d}\sqrt{t}} \tag{A3}$$

which is simply the local slope of $w(t)$ in $t^{1/2}$. The corresponding relationship to physical coefficients may be given as

$$b_{ei}(t) = 2\varrho(t)\alpha_{ei}(t)\Delta T_{ei}(t)\sqrt{\frac{D_{ei}(t)}{\pi}}, \tag{A4}$$

SED
7, 1163–1207, 2015

which has the same form as Eq. (A2), except that physical coefficients are also transient effective properties. In comparison, the seafloor heat flux is

$$q_{\mathrm{sf}}(t) = k \frac{\mathrm{d}T(t)}{\mathrm{d}z}\bigg|_{z=0} \tag{A5}$$

which, for half-space cooling, may be related to properties of the lithosphere as

$$q_{\mathrm{sf}}(t) = [\rho C_p]_{\mathrm{ei}}(t) \Delta T_{\mathrm{ei}}(t) \sqrt{\frac{D_{\mathrm{ei}}(t)}{\pi t}} + q_{\mathrm{a}}, \tag{A6}$$

where q_{a} is the adiabatic part of the heat flux. Moving time to the left hand side, we can define the variable

$$g(t) = [q_{\mathrm{sf}}(t) - q_{\mathrm{a}}]\sqrt{t} = [\rho C_p]_{\mathrm{ei}}(t) \Delta T_{\mathrm{ei}} \sqrt{\frac{D_{\mathrm{ei}}(t)}{\pi}} \tag{A7}$$

which may be referred to as a diminution rate for surface heat flow, analogous to the transient subsidence rate $b_{\mathrm{ei}}(t)$.

From the above it can be seen that the seafloor heat flux is not easily related to net seafloor subsidence or even the net subsidence rate. However, the heat flow diminution rate may be related directly to the transient subsidence rate as

$$\frac{b_{\mathrm{ei}}(t)}{2\varrho(t)\alpha_{\mathrm{ei}}(t)} = \frac{g(t)}{[\rho C_p]_{\mathrm{ei}}(t)}, \tag{A8}$$

which has a similar form to previous derivations of the relationship between the heat content of the lithosphere and seafloor topography (e.g. Parsons and McKenzie, 1978; Sandwell and Poehls, 1980; Wei and Sandwell, 2006).

SED
7, 1163–1207, 2015

Appendix B: Effective thermal properties

If we have a function of many variables $C(z_1(t), z_2(t), \ldots)$, we may find the constant value C_e which, if substituted in an equation in which $C(z_1(t), z_2(t), \ldots)$ appears, would give the same result. For example, the multi-dependent thermal expansivity $\alpha(T, X, P)$ and an amount of temperature change δT in a lithospheric column is related to the displacement of its surface δw as:

$$\delta w = \varrho \int_0^L \alpha(T, P, X) \delta T \, \mathrm{d}z. \tag{B1}$$

where L is the base of the column, X is the composition, P is the pressure, and

$$\varrho = \frac{\rho_\mathrm{b}}{\rho_\mathrm{b} - \rho_\mathrm{wa}} \tag{B2}$$

is the isostatic correction for seawater overburden where ρ_b is the mean density of the mantle column at the ridge axis and ρ_wa is the mean density of the seawater column.

With the effective thermal expansivity α_e we may rewrite the above equation as

$$\delta w = \alpha_\mathrm{e} \varrho \int_0^L \delta T \, \mathrm{d}z. \tag{B3}$$

If the properties T, P, and X change with time, then we may find an effective value for each time such that

$$\frac{1}{\varrho} \frac{\mathrm{d}w}{\mathrm{d}t} = \alpha_\mathrm{ei}(t) \int_0^L \frac{\mathrm{d}T}{\mathrm{d}t} \mathrm{d}z \approx \int_0^L \alpha(T, P, X) \frac{\mathrm{d}T}{\mathrm{d}t} \mathrm{d}z \tag{B4}$$

SED
7, 1163–1207, 2015

can be satisfied, where ≈ indicates an approximate equivalence in the limit of incompressibility, $\mathrm{d}V/\mathrm{d}t \approx 0$, where V is the volume in which we integrate over the dimension z.

The effective thermal expansivity of a cooling lithospheric column is therefore

$$\alpha_{\mathrm{ei}}(t) = \int_0^L \alpha(T,P,X)\frac{\mathrm{d}T}{\mathrm{d}t}\mathrm{d}z \Big/ \int_0^L \frac{\mathrm{d}T}{\mathrm{d}t}\mathrm{d}z, \tag{B5}$$

and the effective volume heat capacity may be found similarly as

$$[\rho C_p]_{\mathrm{ei}}(t) = q_{\mathrm{sf}}(t) \Big/ \int_0^L \frac{\mathrm{d}T}{\mathrm{d}t}\mathrm{d}z, \tag{B6}$$

respectively.

The effective thermal diffusivity and thermal conductivity of the lithosphere may also be calculated, but as it seems to us to be of little substance to the current work and is more involved, it is not discussed here.

Acknowledgements. We thank D. Hasterok for valuable exchanges and clarifications on the details of his work, comments on the statistical analysis of heat flow, and access to his processed data. We are grateful to J. Hillier for providing his database of filtered global seafloor topography. Also thanks to S. Swift for his sediment thickness dataset, and E. Mittelstaedt for critical comments on the Galapagos hotspot. Bicubic splines of sediment thickness and heat flow data used the software package GMT (Wessel and Smith, 1998). D. Muller and L. Husson provided insightful reviews of an early version of this manuscript. The work of J. C. Afonso has been supported by two Australian Research Council Discovery Grants (DP120102372 and DP110104145). This is contribution XXX from the Australian Research Council Centre of Excellence for Core to Crust Fluid Systems (http://www.ccfs.mq.edu.au) and XXX in the GEMOC Key Centre (http://www.gemoc.mq.edu.au).

SED
7, 1163–1207, 2015

References

Afonso, J. C., Ranalli, G., and Fernandez, M.: Density structure and buoyancy of the oceanic lithosphere revisited, Geophys. Res. Lett., 34, L10302, doi:10.1029/2007GL029515, 2007.

Afonso, J.C., Zlotnik, S., Fernandez, M.: Effects of compositional and rheological stratifications on small-scale convection under the oceans: implications for the thickness of oceanic lithosphere and seafloor flattening, Geophys. Res. Lett., 35, doi:10.1029/2008GL035419, 2008.

Becker, K., et al.: Drilling deep into young oceanic crust, hole 504b, Costa Rica rift, Rev. Geophys., 27, 79–102, 1989.

Bodvarsson, G. and Lowell, R. P.: Ocean-floor heat flow and circulation of interstitial waters, J. Geophys. Res., 77, 4472–4475, 1972.

Bullard, E. C.: Discussion of a paper by R. Revelle and A. E. Maxwell, heat flow through the floor of the eastern North Pacific Ocean, Nature, 170, 199–200, 1952.

Chen, Y. J. and Morgan, J. P.: The effects of spreading rate, the magma budget, and the geometry of magma emplacement on the axial heat flux at mid-ocean ridges, J. Geophys. Res., 101, 11475–11482, 1996.

Cherkaoui, A. S. M., Wilcock, W. S. D., Dunn, R. A., and Toomey, D. R.: A numerical model of hydrothermal cooling and crustal accretion at fast spreading mid-ocean ridges, J. Geophys. Res., 101, 11475–11482, 2003.

Cochran, J. R.: Simple models of diffuse extension and pre-seafloor spreading development of the continental margin of the Northeastern Gulf of Aden, Proceedings 26th International Geological Congress, Geology of continental margins symposium, Paris, 7–17 July , Oceanol. Acta, 155–165, 1981.

Cochran, J. R. and Buck, W. R.: Near-axis subsidence rates, hydrothermal circulation, and thermal structure of mid-ocean ridge crests, J. Geophys. Res., 106, 19233–19258, 2001.

Craft, K. L. and Lowell, R. P.: A boundary layer model for submarine hydrothermal heat flows at on-axis and near-axis regions, Geochem. Geophys. Geosy., 10, Q12012, doi:10.1029/2009GC002707, 2009.

Crowley, J. W., Gerault, M., and O'Connell, R. J.: On the relative influence of heat and water transport on planetary dynamics, Earth. Planet. Sci. Lett., 310, 380–388, 2011.

d'Acremont, E., Leroy, S., Maia, M., Gente, P., and Autin, J.: Volcanism, jump and propogation on the Sheba ridge, eastern Gulf of Aden: Segmentation evolution and implications for oceanic accretion processes, Geophys. J. Int., 180, 535–551, 2010.

SED
7, 1163–1207, 2015

Davis, E. E., Fisher, A. T., Firth, J. V., Andersson, E. M., Aoike, K., Becker, K., Brown, K. A., Buatier, M. D., Constantin, M., Elderfield, H., Gonçalves, C. A., Grigel, J. S., Hunter, A. G., Inoue, A., Lawrence, R. M., Macdonald, R. D., Marescotti, P., Martin, J. T., Monnin, C., Mottl, M. J., Pribnow, D. F. C., Stein, J. S., Su, X., Sun, Y.-F., Underwood, M. B., Vanko, D. A., and Wheat, G.: Introduction and Summary: hydrothermal circulation in the oceanic crust and its consequences on the eastern flank of the Juan de Fuca ridge, Proc. Initial Rep. Deep Sea, 168, 7–21, 1997.

Davis, E. E., Chapman, D. S., Wang, K., Villinger, H., Fisher, A. T., Robinson, S. W., Grigel, J., Pribnow, D., Stein, J., and Becker, K.: Regional heat flow variations across the sedimented Juan de Fuca ridge eastern flank: constraints on lithospheric cooling and lateral hydrothermal heat transport, J. Geophys. Res., 104, 17675–17688, 1999.

Davis, E. E., Becker, K., and He, J.: Costa Rica Rift revisited: constraints on shallow and deep hydrothermal circulation in young oceanic crust, Earth Planet Sci. Lett., 222, 863–879, 2004.

Dunn, R. A., Toomey, D. R., and Solomon, S. C.: Three-dimensional seismic structure and physical properties of the crust and shallow mantle beneath the East Pacific Rise at 9°30′ N, J. Geophys. Res., 105, 23537–23555, 2000.

Elderfield, H., Wheat, C. G., Mottl, M. J., Monnin, C., and Spiro, B.: Fluid and geochemical transport through oceanic crust: a transect across the eastern flank of the Juan de Fuca ridge, Earth Planet. Sci. Lett., 172, 151–165, 1999.

Goutorbe, B.: Combining seismically derived temperature with heat flow and bathymetry to constrain the thermal structure of oceanic lithosphere, Earth Planet. Sci. Lett., 295, 390–400, 2010.

Grose, C. J.: Properties of oceanic lithosphere: revised plate model predictions, Earth Planet. Sci. Lett., 333–334, 250–264, 2012.

Grose, C. J. and Afonso, J. C.: Comprehensive plate models for the thermal evolution of oceanic lithosphere, Geochem. Geophys. Geosy., 14, 3751–3778, 2013.

Han, S., Carbotte, S. M., Carton, H., Mutter, J. C., Aghaei, O., Nedimovic, M. R., and Canales, J. P.: Architecture of on- and off-axis magma bodies at EPR 9°37–40′ N and implications for oceanic crustal accretion, Earth. Planet. Sci. Lett., 390, 31–44, 2014.

Hasterok, D.: Thermal regime of the continental and oceanic lithosphere, Ph.D. Dissertation, University of Utah, 156 pp., 2010.

Hasterok, D.: A heat flow based cooling model for tectonic plates, Earth. Planet. Sci. Lett., 311, 386–395, 2013a.

SED
7, 1163–1207, 2015

Hasterok, D.: Global patterns and vigor of ventilated hydrothermal circulation through young seafloor, Earth. Planet. Sci. Lett., 380, 12–20, 2013b.
Hasterok, D., Chapman, D. S., and Davis, E. E.: Oceanic heat flow: implications for global heat loss, Earth. Planet. Sci. Lett., 311, 386–395, 2011.
Hessler, R. R., Smithey, W. M., Boudrias, M. A., Keller, C. H., Lutz, R. A., and Childress, J. J.: Spatial and temporal variation of giant clams, tube worms, and mussels at deep-sea hydrothermal vents, Bull. Biol. Soc. Wash., 6, 411–428, 1988.
Hillier, J. K.: Subsidence of "normal" seafloor: observations do indicate "flattening", J. Geophys. Res., 115, B03102, doi:10.1029/2008JB005994, 2010.
Hobart, M., Langseth, M., and Anderson, R.: A geothermal and geophysical survey of the south flank of the Costa Rica Rift: site 504 and 505, Initial Rep. Deep Sea, 83, 379–404, 1985.
Hofmeister, A. M. and Criss, R. E.: Earth's heat flux revisited and linked to chemistry, Tectonophysics, 395, 159–177, 2005.
Hutnak, M., Fisher, A. T., Harris, R., Stein, C., Wang, K., Spinelli, G., Schindler, M., Villinger, H., and Silver, E.: Large heat and fluid fluxes driven through mid-plate outcrops on ocean crust, Nat. Geosci., 1, 611–614, 2008.
Jannasch, H. W.: Microbial processes at deep-sea hydrothermal vents, in: Hydrothermal Processes at Sea Floor Spreading Centers, edited by: Rona, P. A., Bostrom, K., Laubier, L., and Smith, K. L., 677–709, Plenum Press, New York, 1983.
Jannasch, H. W.: Microbial interactions with hydrothermal fluids, in: Seafloor Hydrothermal Systems, edited by: Humphreis, S. E., Zierenberg, R. A., Mullineaux, L. S., and Thomson, R. E., Geoph. Monog. Series, 91, 273–296, 1995.
Kaul, N., Foucher, J.-P., and Heesemann, M.: Estimating mud expulsion rates from temperature measurements on Hakon Mosby Mud Volcano, SW Barents Sea, Marine Geol., 229, 1–14, 2006.
Langseth M. G., Le Pichon, X., and Ewing, M.: Crustal structure of the mid-ocean ridges, 5, heat flow through the Atlantic Ocean floor and convection currents, J. Geophys. Res., 71, 5321, doi:10.1029/JZ071i022p05321, 1966.
Langseth, M. G., Mottl, M. J., Hobart, M. A., and Fisher, A. T.: The distribution of geothermal and geochemical gradients near Site 501/504: implications for hydrothermal circulation in the oceanic crust, Proc. Ocean Drill. Prog., Sci. Results 111, 23–32, 1988.
Le Pichon, X.: Sea-floor spreading and continental drift, J. Geophys. Res., 73, 12, 3661–3697, 1968.

SED
7, 1163–1207, 2015

Leroy, S., et al.: From rifting to oceanic spreading in the Gulf of Aden: a synthesis, Front. Earth Sci., 2, 385–427, 2012.
Lister, C. R. B.: On the penetration of water into hot rock, Geophys. J. Roy. Astron. Soc., 39, 465–509, 1974.
Lister, C. R. B.: "Active" and "Passive" hydrothermal systems in the ocean crust, predicted physical conditions, in: The Dynamic Environment of the Ocean Floor, edited by: Fanning, K. A. and Manheim, F. T., Heath, Lexington, MA, 441–470, 1982.
Lowell, R. P. and Rona, P. A.: Seafloor hydrothermal systems driven by the serpentinization of peridotite, Geophys. Res. Lett., 29, 1531, doi:10.1029/2001GL014411, 2002.
Lucazeau, F. et al.: Persistent thermal activity at the Eastern Gulf of Aden after continental break-up, Nat. Geosci., 1, 854–858, 2008.
Lucazeau, F., Leroy, S., Rolandone, F., d'Acremont, E., Watremez, L., Bonneville, A., Goutorbe, B., and Dusunur, D.: Heat-flow and hydrothermal circulation at the ocean-continent transition of the eastern gulf of Aden, Earth. Planet. Sci. Lett., 295, 554–570, 2010.
Maclennan, J. T.: The supply of heat to mid-ocean ridges by crystallization and cooling of mantle melts, in: Magma to Microbe: Modeling Hydrothermal Processes at Oceanic Spreading Centers, edited by: Lowell, R. P., Seewald, J. S., Metaxas, A., and Perfit, M. R., Geophysical Monograph 178, American Geophysical Union, Washington, DC, 2008.
McKenzie, D. P.: Some remarks on heat flow and gravity anomalies, J. Geophys. Res., 72, 6261–6273, 1967.
McKenzie, D. P. and Parker, R. L.: The North Pacific: an example of tectonics on a sphere, Nature, 216, 1276–1280, 1967.
McKenzie, D., Jackson, J., and Priestley, K.: Thermal structure of oceanic and continental lithosphere, Earth. Planet. Sci. Lett., 233, 337–349, 2005.
Mottl, M. J.: Partitioning of energy and mass fluxes between mid-ocean ridge axes and flanks at high and low temperature, in: Energy and Mass Transfer in Marine Hydrothermal Systems, edited by: Halbach, P. E., Tunnicliffe, V., and Hein, J. R., 271–286, 2003.
Muller, R. D., et al.: Digital isochrones of the world's ocean floor, J. Geophys. Res., 102, 3211–3214, 1997.
Muller, R. D., Sdrolias, M., Gaina, C., and Roest, W. R.: Age, spreading rates and spreading symmetry of the world's ocean crust, Geochem. Geophys. Geosy., 9, Q04006, doi:10.1029/2007GC001743, 2008.

SED
7, 1163–1207, 2015

Nedimovic, M. R., Bohnenstiehl, D. R., Carbotte, S. M., Canales, J. P., and Dziak, R. P.: Faulting and hydration of the Juan de Fuca plate system, Earth. Planet. Sci. Lett., 284, 94–102, 2009.
Newman, K. R., Nedimovic, M. R., Canales, J. P., and Carbotte, S. M.: Evolution of seismic layer 2B across the Juan de Fuca ridge from hydrophone streamer 2-D traveltime tomography, Geochem. Geophys. Geosy., 12, Q05009, doi:10.1029/2010GC003462, 2011.
Parsons, B. and McKenzie, D.: Mantle convection and the thermal structure of the plates, J. Geophys. Res., 83, 4485–4496, 1978.
Pelayo, A. M., Stein, S., and Stein, C. A.: Estimation of oceanic hydrothermal heat flux from heat flow and depths of midocean ridge seismicity and magma chambers, Geophys. Res. Lett., 21, 713–716, 1994.
Pribnow, D. F. C., Davis, E. E., and Fisher, A. T.: Borehole heat flow along the eastern flank of the Juan de Fuca ridge, including effects of anisotropy and temperature dependence of sediment thermal conductivity, J. Geophys. Res., 105, 13449–13456, 2000.
Rosenberger, A., Davis, E. E., and Villinger, H.: Data report: Hydrocell-95 and -96 single-channel seismic data on the eastern Juan de Fuca ridge flank, Proc. Ocean Drill. Prog., Sci. Results, 168, 9–19, 2000.
Ryan, J. G. and Chauvel, C. C.: The subduction zone conveyor and the impact of recycled materials on the evolution of the mantle, Chap. 2.11, the mantle and core, in: Treatise on Geochemistry, 2nd edn., edited by: Carlson, R., 2013.
Sandwell, D. T. and Poehls, K. A.: A compensation mechanism for the central Pacific, J. Geophys. Res., 85, 3751–3758, 1980.
Schmidt, M. W. and Poli, S.: Devolitization during subduction, the crust, in: Treatise on Geochemistry, 2nd edn., 669–701, 2013.
Sclater, J. G.: Variability of heat flux through the seafloor: discovery of hydrothermal circulation in the oceanic crust, in: Hydrogeology of the Oceanic Lithosphere, edited by: Davis, E. E. and Elderfield, H., Cambridge University Press, 2004.
Sclater, J. G. and Francheteau, J.: The implications of terrestrial heat flow observations on current tectonic and geochemical models of the crust and upper mantle of the Earth, Geophys. J. R. Astr. Soc., 20, 509–542, 1970.
Sclater, J. G., Anderson, R. N., and Bell, M. L.: Elevation of ridges and evolution of the central eastern Pacific, J. Geophys. Res., 76, 7888–7915, 1971.
Sclater, J. G., Jaupart, C., and Galson, D.: The heat flow through oceanic and continental crust and the heat loss of the Earth, Rev. Geophys. Space Phys., 18, 269–311, 1980.

SED
7, 1163–1207, 2015

Seyfried, W. E., Janecky, D. R., and Mottl, M. J.: Alteration of the oceanic crust: implications for geochemical cycles of lithium and boron, Geochim. Cosmochim. Acta, 48, 557–569, 1984.
Sleep, N. H.: Sensitivity of heat flow and gravity to the mechanism of sea-floor spreading, J. Geophys. Res., 74, 542–549, 1969.
Smith, W. H. F. and Sandwell, D. T.: Global sea floor topography from satellite altimetry and ship depth soundings, Science, 277, 1956–1962, 1997.
Spinelli, G. A. and Harris, R. N.: Effects of the legacy of axial cooling on partitioning of hydrothermal heat extraction from oceanic lithosphere, J. Geophys. Res., 116, B09102, doi:10.1029/2011JB008248, 2011.
Spivack, A. J. and Edmond, J. M.: Boron isotopic exchange between seawater and the oceanic crust, Geochim. Cosmochim. Acta, 51, 1033–1043, 1987.
Staudigel, H.: Chemical fluxes from hydrothermal alteration of oceanic crust, Chapter 4.16, the crust, in: Treatise on Geochemistry, 2nd edn., 2014.
Stein, C. A. and Stein, S.: A model for the global variation in oceanic depth and heat flow with lithospheric age, Nature, 359, 123–129, 1992.
Stein, C. A. and Stein, S.: Constraints on Pacific midplate swells from global depth-age and heat flow-age models, in: The Mesozoic Pacific: Geology, Tectonics, Volcanism. American Geophyscial Union Geophysical Monograph 77, 1993.
Stein, C. A., and Stein, S.: Constraints on hydrothermal heat flux through the oceanic lithosphere from global heat flow, J. Geophys. Res., 99, 3081–3095, 1994.
Stein, C. A., Stein, S., and Pelayo, A. M.: Heat flow and hydrothermal circulation, in: Seafloor Hydrothermal Systems: Physical, Chemical, Biological and Geological Interactions, edited by: Humphris, S. E. et al., American Geophysical Union, Washington, DC, 425–445, 1995.
Swift, S. A., Kent, G. M., Detrick, R. S., Collins, J. A., and Stephen, R. A.: Oceanic basement structure, sediment thickness, and heat flow near Hole 504B, J. Geophys. Res., 103, 15377–15391, 1998.
Theissen-Krah, S., Lyer, K., Rupke, L. H., and Morgan, J. P.: Coupled mechanical and hydrothermal modeling of crustal accretion at intermediate to fast spreading ridges, Earth Planet. Sci. Lett., 311, 275–286, 2011.
Tunnicliffe, V.: The biology of hydrothermal vents: ecology and evolution, Oceanogr. Mar. Biol. Annu. Rev., 29, 319–407, 1991.
Von Herzen, R. P.: Heat flow values from the South-Eastern Pacific, Nature, 183, 882–883, 1959.

SED
7, 1163–1207, 2015

Von Herzen, R. and Uyeda, S.: Heat flow through the eastern Pacific ocean floor, J. Geophys. Res., 68, 4219–4250, 1963.
Von Herzen, R. P., Davis, E. E., Fisher, A. T., Stein, C. A., and Pollack, H. N.: Comments on "Earth's heat flux revisited and linked to chemistry" by A. M. Hofmeister and R. E. Criss, Tectonophysics, 409, 193–198, 2005.
Wei, M. and Sandwell, D.T.: Estimates of heat flow from Cenozoic seafloor using global depth and age data, Tectonophysics, 417, 325–335, 2006.
Wessel, P. and Smith, W. H. F.: New, improved version of the Generic Mapping Tools released, EOS Trans. AGU, 79, 579, doi:10.1029/98EO00426, 1998.
Wheat, C. G., Mottl, M. J., Fisher, A. T., Kadko, D., Davis, E. E., and Baker, E.: Heat flow through a basaltic outcrop on a sedimented young ridge flank, Geochem. Geophys. Geosy., 5, Q12006, doi:10.1029/2004GC000700, 2004.
Wilson, D. S. and Hey, R. N.: History of rift propogation and magnetization intensity for the Cocos-Nazca spreading center, J. Geophys. Res., 100, 10041–10056, 1995.

SED
7, 1163–1207, 2015

Table 1. Comparison of heat flow deficit estimates for different seafloor domains for this study compared to previous studies.

Model	Active Deficit	Flank Deficit	Near-Axial Deficit	Passive Deficit	Total Deficit
This Study: Mode(TW (% of total))					
H13	1.1(14 %)	1.4(18 %)	2.5(32 %)	5.3(68 %)	7.8
GH	4.4(44 %)	0.8(8 %)	5.2(52 %)	4.8(48 %)	10.0
GHC	2.8(42 %)	0.5(18 %)	3.3(49 %)	3.3(51 %)	6.6
This Study: Median(TW(% of total))					
H13	0.7(11 %)	0.9(14 %)	1.6(24 %)	5.0(76 %)	6.6
GH	3.7(42 %)	0.7(8 %)	4.4(49 %)	4.5(51 %)	8.9
GHC	2.2(39 %)	0.4(7 %)	2.6(46 %)	3.1(54 %)	5.7
This Study: Mean(TW(% of total))					
H13	0.5(8 %)	0.6(10 %)	1.1(18 %)	4.9(82 %)	6.0
GH	3.3(40 %)	0.6(7 %)	3.9(47 %)	4.4(53 %)	8.3
GHC	1.7(32 %)	0.3(6 %)	2.0(38 %)	3.3(62 %)	5.3
Previous Studies (TW(% of total))*					
SS94	–	–	3.2(28 %)	8.1(72 %)	11.3
P94	–	–	2.2(23 %)	7.2(77 %)	9.4
M03	2.0(20 %)	0.8 (8 %)	2.8(28 %)	7.1(71 %)	9.9
SH11C	–	–	2.0(25 %)	6.0(75 %)	8.0**
SH11H	–	–	3.6(40 %)	5.4(60 %)	9.0
H13U	–	–	2.3(37 %)***	3.9(63 %)***	6.2
H13SF	–	–	2.3(29 %)***	5.5(71 %)***	7.8

* SS94 – Stein and Stein (1994), P94 – Pelayo et al. (1994), M03 – Mottl (2003), SH11C – Conduction-only model of Spinelli and Harris (2011), SH11H – Hydrothermally corrected conduction model of Spinelli and Harris (2011), H13U – Hasterok (2013b) using his unfiltered heat flow database, H13SF – Hasterok (2013b) using his sediment-filtered heat flow database. ** Based on Spinelli and Harris's (2011) assertion that hydrothermal circulation does not change total hydrothermal power. *** Estimated based on inspection of figures in Hasterok (2013b).

SED
7, 1163–1207, 2015

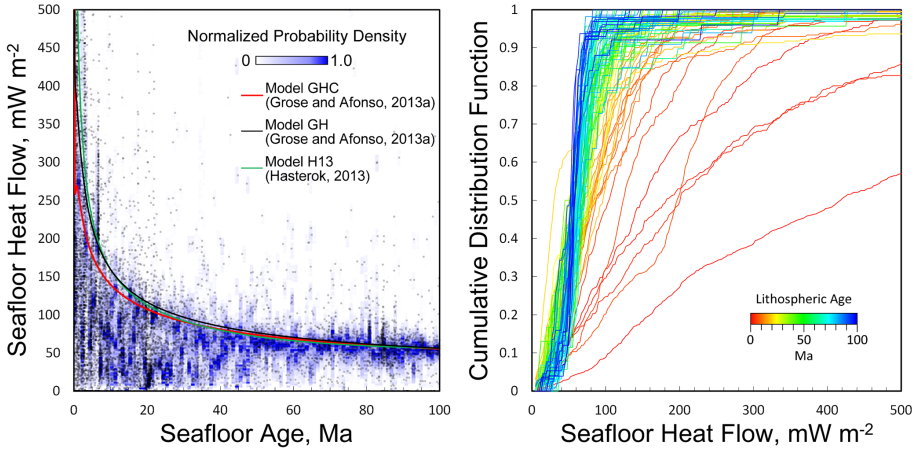

Figure 1. (a) Heat flow measurements used in this study (black dots) and normalized probability density of heat flow constructed from the data, compared to the three thermal plate models used in this study. **(b)** Cumulative distribution functions of heat flow in 1 Ma bins between 1 and 100 Ma.

SED
7, 1163–1207, 2015

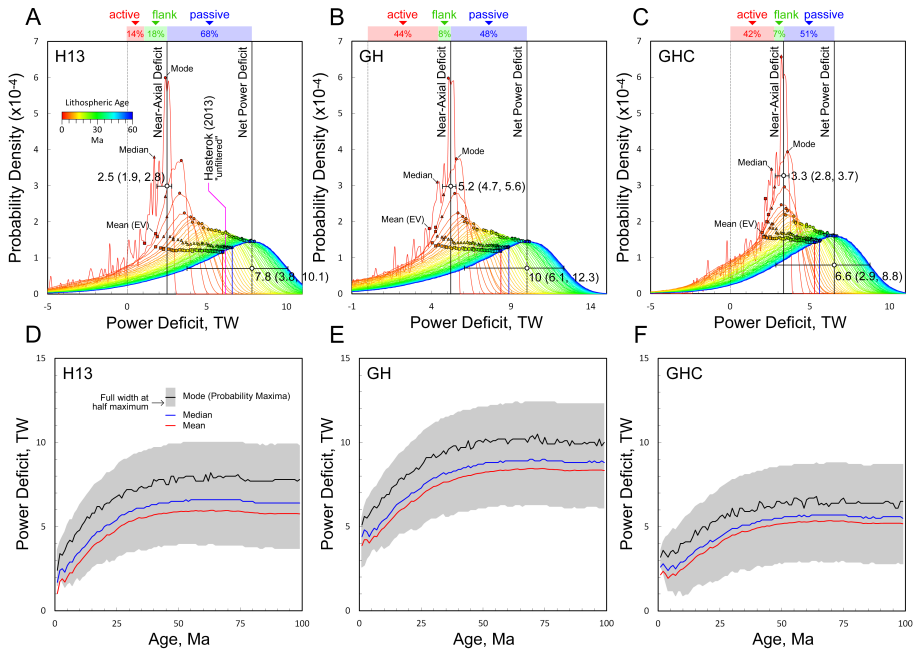

Figure 2. Probability density functions of the heat flow deficit determined from monte carlo analysis for models **(a)** H13 (Hasterok 2013a), **(b)** GH, and **(c)** GHC (Grose and Afonso, 2013). Each PDF represents numerical integration to 1,2–60 Ma with color indicating final time of integration. Colored circles, triangles, and squares indicate the mode, median, and mean of their respective PDF's. The large white circles with error bars indicate the mode and half-maximum bounds for the 1 Ma (near-axial power deficit) and 60 Ma (net power deficit) PDF's. The red, green, and blue bars above the graphs indicate the fraction of active, flank, and passive advective power, respectively. Hasterok's (2013b) "unfiltered" estimate is indicated in panel **(a)**. Bottom panels show the mean, median, mode, and half-maximum uncertainty of the power deficit as a function of age for the above respective models.

SED
7, 1163–1207, 2015

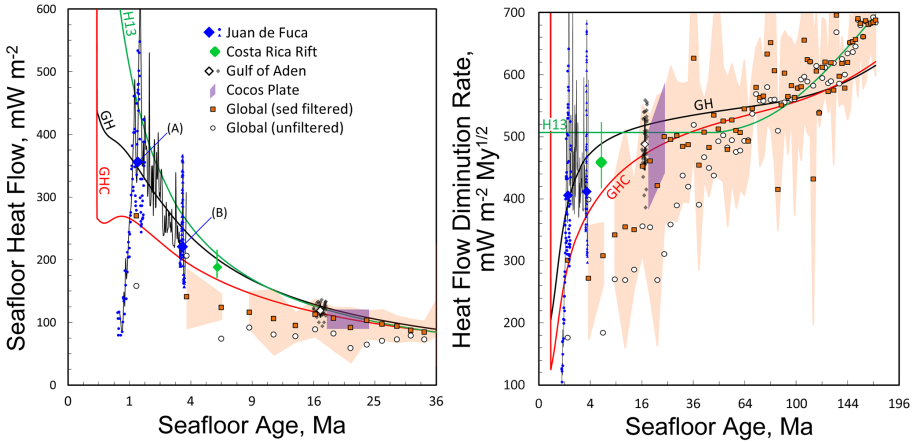

Figure 3. Predicted heat flow **(a)** and heat flow diminution rate **(b)** for models H13, GH, and GHC as a function of age compared with global and site-specific data. The site-specific data-points are discussed in the text. The global sediment filtered and unfiltered data shown here are from Hasterok (2013b). The highlighted region is the uncertainty (1σ) of the sediment-filtered global dataset. Note that the misfit between models GHC and the data occurs because Grose and Afonso (2013) fitted model GHC to heat flow data which did not include a correction for thermal rebound in the continuously thickening sediment column.

SED
7, 1163–1207, 2015

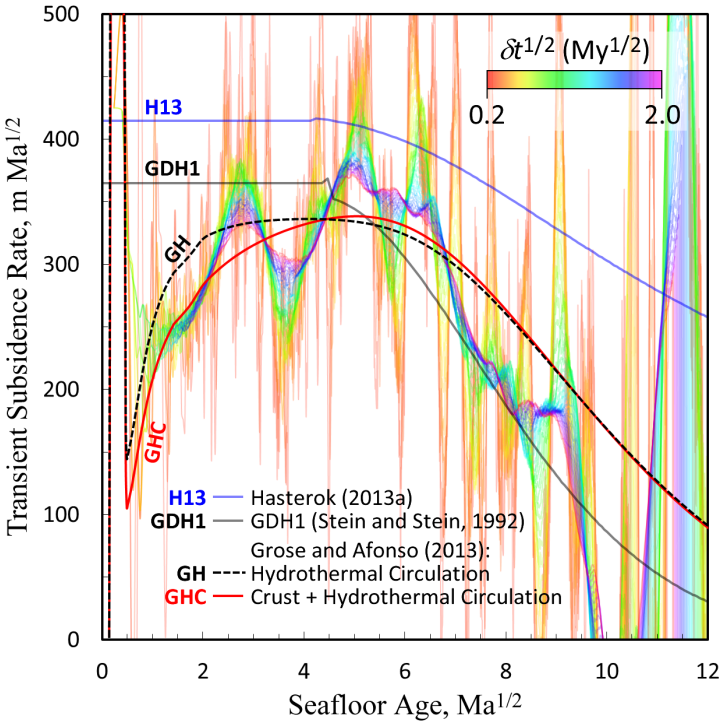

Figure 4. Subsidence rates for models GH and GHC from Grose and Afonso (2013) and the classical model GDH1 (Stein and Stein, 1992) compared with subsidence rates estimated from the global depth dataset of Hillier (2010). Red-yellow colors correspond to small sliding windows and blue-violet colors correspond to large sliding windows over which subsidence rates are determined using a least-squares fit. The small discontinuities around 20 Ma for GHD1 and H13 are due to the imperfect fit their author's respective equations for seafloor depth. See text for discussion.

SED
7, 1163–1207, 2015

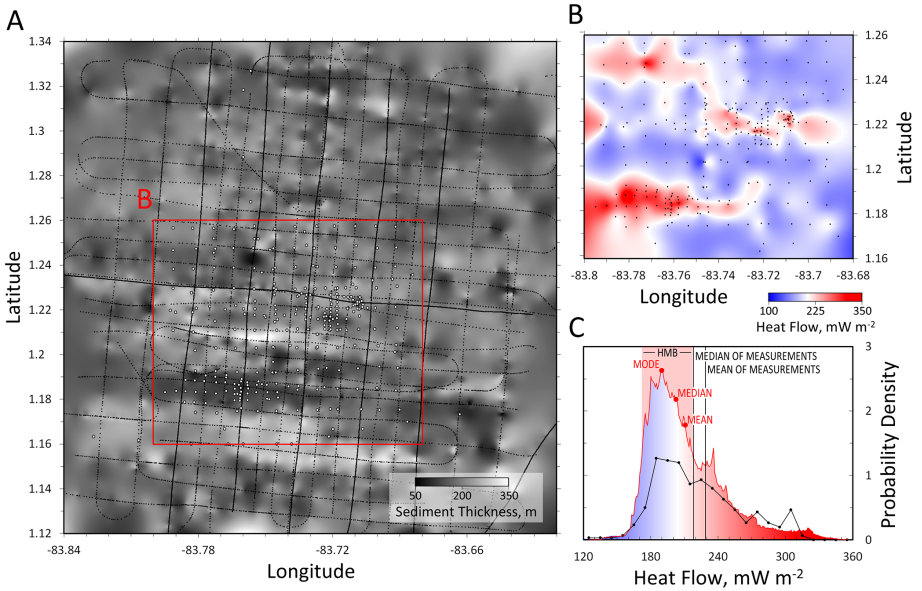

Figure 5. (a) Sediment thickness map constructed from a bicubic spline of seismic reflection profiles (dotted line, where dots are datapoints; Swift et al., 1998). Open circles are sites of heat flow measurement. **(b)** Heat flow map constructed from a bicubic spline of measurements (black dots). **(c)** Non-normalized Probability density functions (PDF) of heat flow. The red PDF is from the bicubic spline in panel **(c)**, whereas the black line is the PDF using only measurements.

SED
7, 1163–1207, 2015

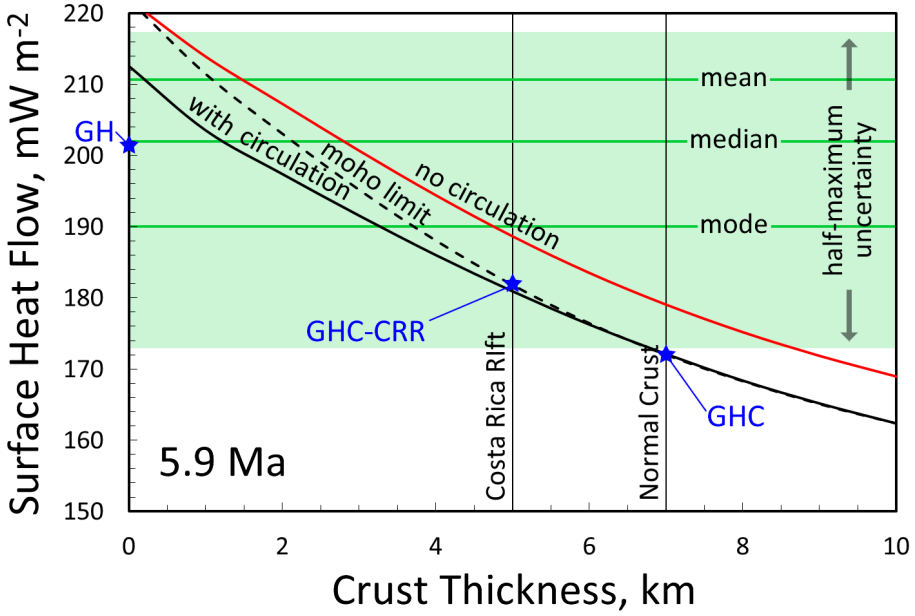

Figure 6. Predicted seafloor heat flow for model GHC with varied crust thickness and parameters affecting hydrothermal circulation are varied, compared to measured heat flow (mean, median, mode, and half-maximum bounds) for the Costa Rica Rift (Fig. 5). The black line is model GHC with oceanic crust varied between 0 and 10 km. The black dashed line is the same model, except hydrothermal circulation is not allowed to occur below the insulating layer. The red line is model GHC with the thickness of oceanic crust varied and no hydrothermal circulation on the ridge axis. All predictions are for 5.9 Ma seafloor.

SED
7, 1163–1207, 2015

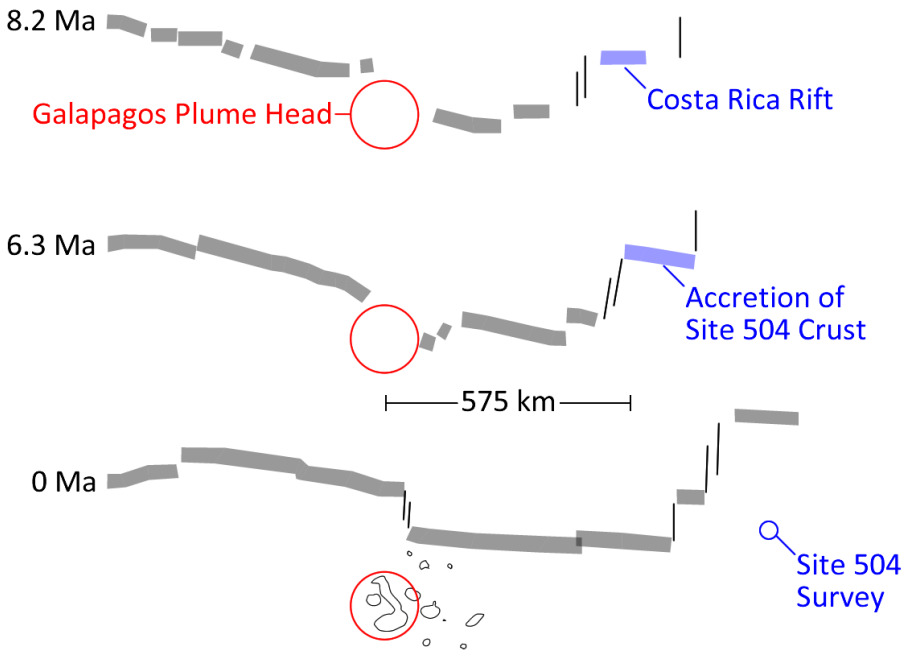

Figure 7. Paleoridge and hotspot placement reconstruction after Wilson and Hey (1995). The locations of the Galapagos "plume head", present-day Site 504 survey, ridge at which Site 504 crust was accreted, and the Costa Rica Rift ridge at 8.2 Ma, are indicated.

SED
7, 1163–1207, 2015